DE GRUYTER OPEN

Journal of ELECTRICAL ENGINEERING, VOL 67 (2016), NO5, 311–322

A NOVEL CURRENT–MODE HIGH–FREQUENCY POLYPHASE FILTER USING MULTI–OUTPUT CURRENT DIFFERENCING TRANSCONDUCTANCE AMPLIFIERS

Hao Peng — Chunhua Wang — Xiaotong Tian *

This paper introduces a novel polyphase filter working at high centre frequency using multi-output current differencing transconductance amplifiers (MOCDTAs). The MOCDTA possesses characteristics of low input impedance, high output impedance, wide work frequency and linearly adjustable transconductance. The proposed filter consists of two MOCDTAs, two grounded capacitors, and no resistors. The features of low input impedance and high output impedance make it suitable for cascade. The bandwidth and centre frequency could be adjusted independently by external bias voltage V_C and V_{Ca}. The image rejection ratio (IRR) could reach 31.6 dB at the centre frequency of 114 MHz, and its bandwidth could be 11.1 MHz. Besides, the centre frequency could be tuned from 38 MHz to 150 MHz with bandwidth of 20.1 MHz. Simulation results which verify the theory are included.

K e y w o r d s: current-mode, analogue circuits, polyphase filter, image rejection, independently tunable, MOCDTA

1 INTRODUCTION

The image interference is an important problem in radio frequency (RF) receivers [1]. To suppress image, some methods have been proposed. Two famous architectures for image rejection have been introduced by Hartley [2] and Weaver [3]. In those above architectures, two separate filters are used in I-path and Q-path, respectively. Both of them are sensitive to mismatch [4, 5]. To compensate the mismatch, various calibration techniques were utilized while increasing the complexity of the circuits [6]. In low-IF receivers, the use of a single polyphase filter is better than the employ of two separate filters [7].

The polyphase filter is an important portion in low-IF receivers. Polyphase filters, known as complex filters, are widely used for image rejection [8, 9]. In order to cascade conveniently, active polyphase filters rather than the passive polyphase filters are widely used [10]. Another advantage is that the active polyphase filter is more suitable for monolithic integration [11].

In all kinds of implementation of the polyphase filter, cascading of the first-order polyphase filter, which could achieve high image rejection, is a simple and convenient approach. However, there is a problem that the polyphase filter based on some active components is unsuitable for high centre frequency. So, design of the first-order polyphase filter is pivotal. Recently, many kinds of active components are utilized to design polyphase filters, such as operational amplifiers (OPAMP) [6, 12], operational transconductance amplifiers (OTA) [13–17], current mirrors [18, 19], second generation current conveyor (CCII) [1, 10, 20–22], current followers (CF) [23], current feedback operational amplifiers (CFOA) [24–26], and current differencing buffered amplifiers (CDBA) [11]. However, polyphase filters based on OPAMP have some disadvantages, such as the limited bandwidth due to the constant gain-bandwidth product and the limited slew rate. OTA-based circuits and CCII-based circuits could reduce these above disadvantages expediently [27, 28]. Nevertheless, a problem still exists in above circuits. The centre frequency of these polyphase filters based on OTAs could not be very high. The reason is that input ports of the OTA are not connected to virtual ground. Likewise, Polyphase filters based on CCIIs suffer from the same problem. Recently, CDBA is also used to realize the polyphase filter. However, CDBA does not have external bias currents, so the parameters of the filter could not be adjusted flexibly. In addition, the structure of polyphase filters using these components is some complicated. In above first-order filters, resistors, which would increase the complexity of the structure and add the source of mismatch, are needed between the two paths to increase the image rejection ratios (IRRs). These above problems limit the use of the active polyphase filter [29].

In 2003, a new current-mode active element, called current differencing transconductance amplifier (CDTA), was introduced [30], and designs using CDTAs have attracted more attentions [31–33]. The CDTA has high output impedance, but it has only two output ports which are not enough for multiple feedback paths of the polyphase filter, and the CDTA is likely to lose the high output impedance because of the feedback. Based on the CDTA, the MOCDTA is introduced, which adds output ports to satisfy more feedbacks without sacrificing the high output impedance. As the same as the CDTA, the MOCDTA possesses input ports of virtual ground, which could work at high frequency. Besides, instead of resistors which are between two paths in the polyphase filter based on

* College of Computer Science and Electronic Engineering, Hunan University, Changsha, China
Corresponding author: Chunhua Wang, devin7960@gmail.com

DOI: 10.1515/jee-2016-0046, Print (till 2015) ISSN 1335-3632, On-line ISSN 1339-309X

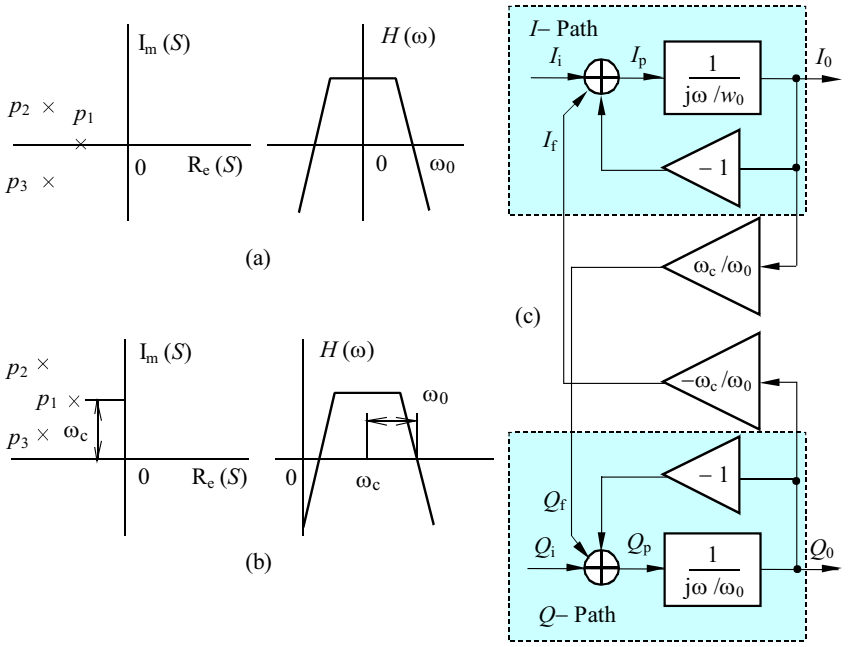

Fig. 1. (a) — The s plane and the amplitude-frequency responses of the low-pass filter; (b) — The s plane and the amplitude-frequency responses of the band-pass complex filter; (c) — the realization of a first-order (single stage) polyphase filter

CDBA, transconductance which could be adjusted by external bias voltage can be used to increase IRR. So, the MOCDTA is suitable for the realization of the polyphase filter for high centre frequency.

In this paper, a novel active polyphase filters using MOCDTAs are presented. The proposed filter consists of two MOCDTAs, two grounded capacitors, and no resistors. Because of low input impedance and high output impedance, this filter is suitable for cascade, which could improve the image rejection.

2 POLYPHASE FILTER THEORY FOR IMAGE REJECTION

2.1 Realization of polyphase filter

The linear frequency transformation is used to achieve the polyphase filter. The transfer function of the low-pass filter can be written as

$$H_{lp}(j\omega) = \frac{1}{1 + j\omega/\omega_0} \tag{1}$$

where ω_0 is the cut-off frequency.

The transformation of the low-pass filter is shown in Fig. 1. Figure 1(a) denotes the s plane and the amplitude-frequency response of the third-order low-pass filter. The poles of this filter are symmetric with the real axis or on the real axis, the response to positive frequency is the same as the one to negative frequency. Figure 1(b) shows the s plane and the amplitude-frequency response of the third-order band-pass complex filter. By shifting the poles up the imaginary axis by ω_C, the low-pass response is transformed into an identical band-pass response centred at ω_C. The resultant band-pass transfer function will be different for positive and negative frequencies. The transfer function of the band-pass complex filter is written as

$$H_{bp}(j\omega) = \frac{1}{1 + (j\omega - j\omega_c)/\omega_0} \tag{2}$$

where ω_C is the centre frequency.

The image rejection ratio (IRR), which was firstly introduced by Norgaard [34], is defined as the ratio of the gain of the desired sideband to the suppression of the image sideband [35]. Using the (2), the IRR can be expressed as

$$IRR(j\omega) = \frac{|H_{bp}(j\omega)|}{|H_{bp}(-j\omega)|} = \frac{\sqrt{\omega_0^2 + (\omega_c + \omega)^2}}{\sqrt{\omega_0^2 + (\omega_c - \omega)^2}} \tag{3}$$

and at $\omega = \omega_C$

$$IRR(j\omega) = \sqrt{1 + 4\frac{\omega_C^2}{\omega_0^2}}, \quad Q = \frac{\omega_C^2}{2\omega_0^2}. \tag{4,5}$$

Next, we can get the realization of the first-order polyphase filter. Firstly, (2) could be rewritten as

$$H_{bp}(j\omega) = H_r(j\omega) + jH_i(j\omega) \tag{6}$$

where $H_r(j\omega)$ and $H_i(j\omega)$ are the real and imaginary parts of (2). They are written by

$$H_r(j\omega) = \frac{1 + j\omega/\omega_0}{4Q^2 + (1 + j\omega/\omega_0)^2}, \tag{7}$$

$$H_i(j\omega) = \frac{2Q}{4Q^2 + (1 + j\omega/\omega_0)^2}. \tag{8}$$

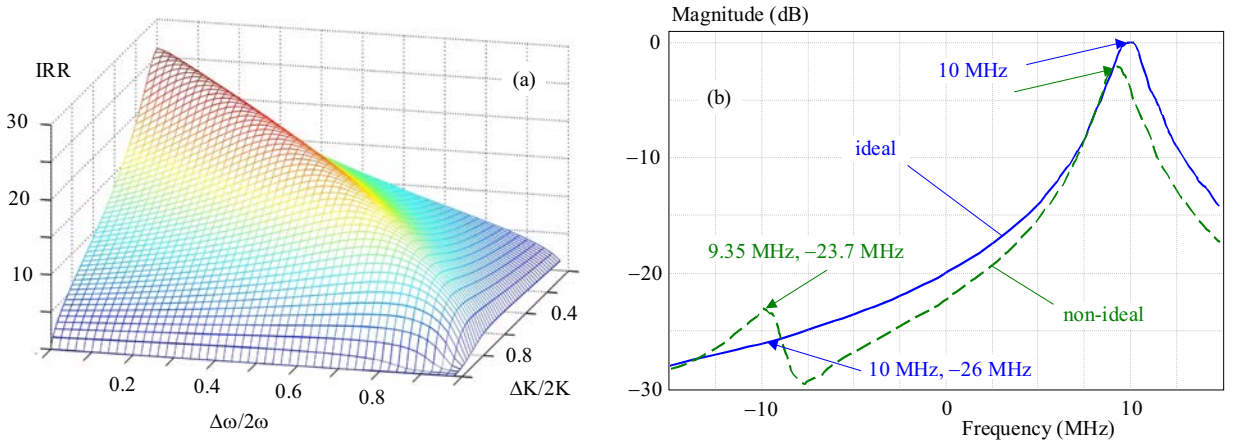

Fig. 2. The effect of mismatch: (a) — IRR with variational values of $\Delta\omega$ and ΔK; (b) — amplitude-frequency response affected by mismatch

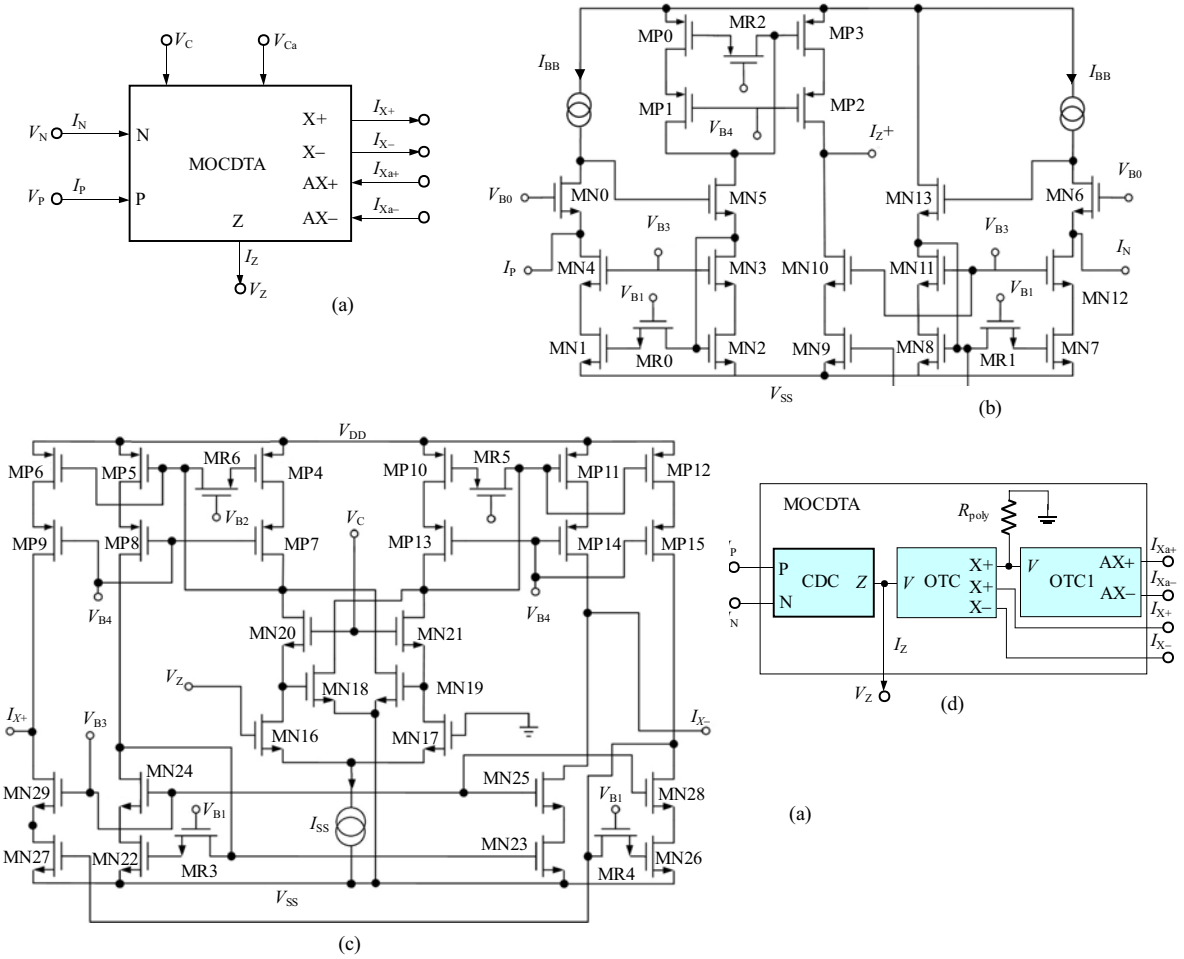

Fig. 3. The symbol and structure of MOCDTA: (a) — symbol of MOCDTA; (b) — current differencing circuit; (c) — operational transconductance circuit; (d) — the configuration of MOCDTA

The input complex signal $f_{in}(j\omega) = f_{inr}(j\omega) + jf_{ini}(j\omega)$ after passing the polyphase filter gives

$$f_{out}(j\omega) = f_{in}(j\omega)H(j\omega) = f_{outr}(j\omega) + jf_{outi}(j\omega)\,, \quad (9)$$

$$f_{outr}(j\omega) = H_r(j\omega)f_{inr}(j\omega) - H_i(j\omega)f_{ini}(j\omega)\,, \quad (10)$$

$$f_{outi}(j\omega) = H_r(j\omega)f_{ini}(j\omega) + H_i(j\omega)f_{inr}(j\omega)\,. \quad (11)$$

Substituting (7) and (8) into (10) and (11), respectively, we can get the equations

$$f_{outr}(j\omega) = \frac{\omega_0}{j\omega}\left[f_{inr}(j\omega) - f_{outr}(j\omega) - \frac{\omega_C}{\omega_0}f_{outi}(j\omega)\right], \quad (12)$$

$$f_{outr}(j\omega) = \frac{\omega_0}{j\omega}\left[f_{inr}(j\omega) - f_{outr}(j\omega) - \frac{\omega_C}{\omega_0}f_{outi}(j\omega)\right], \quad (13)$$

the input and output of the I-path are f_{inr} and f_{outr}, and the input and output of the Q-path are f_{ini} and f_{outi}, respectively. So, the realization of the polyphase filter is given in Fig. 1(c). In Fig. 1(c), I_i and Q_i are the inputs which have equal amplitudes and 90-degree phase difference between the I-path and Q-path. I_o and Q_o are the outputs, I_f and Q_f are feedback signals between two paths. It is observed that that the polyphase is made up of close cross-coupling of two equal real low-pass filters.

2.2 Influence of Mismatch

When the I-path and Q-path are perfectly matched, it can achieve the best IRR. However, the mismatch of components is unavoidable. So, the cut-off frequencies ω_{i0} and ω_{q0} of I and Q path could not be equal. Besides, the constant gain ω_C/ω_0 of feedbacks exist mismatch. K is defined as ω_C/ω_0, K_i and K_q are K with mismatch between I and Q path. With mismatch $\Delta\omega$ and ΔK, the ω_{i0}, ω_{q0}, K_i, and K_q could be written as follows

$$\omega_{i0} = \omega_0\big(1 - \frac{\Delta\omega}{2\omega}\big),\ \ \omega_{q0} = \omega_0\big(1 + \frac{\Delta\omega}{2\omega}\big), \tag{14}$$

$$K_i = K\big(1 - \frac{\Delta K}{2K}\big),\ \ K_q = K\big(1 + \frac{\Delta K}{2K}\big) \tag{15}$$

and the transfer function with mismatch could be written as

$$H_{\text{bp\_with\_mismatch}}(j\omega) = \frac{\omega_{i0}\omega_{q0} + j(\omega_{i0}\omega + \omega_{i0}\omega_{q0}K_i)}{\omega_{i0}\omega_{q0} + K_iK_q\omega_{i0}\omega_{q0} - \omega^2 + j(\omega_{i0}\omega + \omega_{q0}\omega)}. \tag{16}$$

Theoretical model has been operated to measure the IRR affected by the mismatch, results are shown in Fig. 2(a) with variational values of $\Delta\omega$ and ΔK. Compared with the ideal one, the simulated amplitude-frequency response with $\Delta\omega/\omega = 20\,\%$ and $\Delta K/2K = 30\,\%$ is shown in Fig. 2(b). The IRR without mismatch could achieve 26.0 dB with $K = 20$ and $\omega_0 = 0.5$ MHz, while the one with the mismatch is only 21.3 dB. The centre frequency also drifts by 0.65 MHz due to the mismatch.

3 CIRCUIT OF MOCDTA

The electrical symbol of the MOCDTA is shown in Fig. 3(a). The MOCDTA has low-impedance current-input ports P and N, and high output-impedance ports Z and X. The input ports can be deemed to connect to virtual ground. The MOCDTA can be characterized by the following equations

$$\begin{gathered} V_P = V_N = 0\,,\ I_Z = I_P - I_N\,,\ V_Z = I_Z Z_Z\,, \\ I_{X+} = g_m V_Z\,,\ I_{X-} = -g_m V_Z\,, \\ I_{Xa+} = KaI_{X+}\,,\ I_{Xa-} = KaI_{X-} \end{gathered} \tag{17}$$

where P and N are input ports, Z and ±X are output ports, g_m is the transconductance gain from port Z to port X, Ka is the current gain from port X± to port AX± and Z_Z is external impedance connected to the port Z. In Fig. 3(a), g_m could be adjusted by the bias voltage V_C, and Ka could be tuned by the bias voltage V_{Ca}. The MOCDTA contains current differencing circuit and operational transconductance circuit mainly, which are shown in Fig. 3(b) and Fig. 3(c). The detail configuration of MOCDTA is shown in Fig. 3(d).

3.1 Current Differencing Circuit

Figure 3(b) shows the current differencing circuit (CDC). In Fig. 3(b), there are two high speed current differencing circuits which are made up of two unity-gain current amplifiers. In the CDC, MN1-MN4, MN7-MN12, and MP0-MP3 are the low-voltage (high-swing) cascade current mirrors. The source of MN0 and MN6 are input ports which are set to be virtual-grounded with the constant IBB and VB0. MN5, MN0 and MN13, MN6 generate negative feedbacks in two input signal paths, respectively, which could make the input resistance lower.

Considering the non-ideal condition, the output current IZ could be writen as

$$I_Z = \alpha_{Pa}I_P - \alpha_{Na}I_N \tag{18}$$

where

$$\alpha_{Pa} = \Big[1 - \frac{g_{mN5,13} + g_{mN1,7}}{g_{mN5,13}g_{mN1,7}(r_o + r_{oB})}\Big] \times \frac{2 + r_o(g_{mP1})}{g_{mP0}[1 + g_{mP1}r_o]}\,\frac{g_{mP3}[1 + g_{mP2}r_o]}{2 + r_o g_{mP2}}, \tag{19}$$

$$\alpha_{Na} = \Big[1 - \frac{g_{mN5,13} + g_{mN1,7}}{g_{mN5,13}g_{mN1,7}(r_o + r_{oB})}\Big] \times \frac{1}{g_{mN1,7}}\,\frac{g_{mN9}[1 + g_{mN10}r_o]}{2 + r_o g_{mN10}} \tag{20}$$

where g_{mNX} and g_{mPX} denote the transconductance of $MNX\,(X = 1,\ 5,\ 7,\ 10,\ 13)$ and $MPX\,(X = 1, 2)$, respectively. r_o and r_{oB} represent the output of transistors and the current sources. With the condition $r_{oB} \gg r_o$, the input resistance could be given as

$$R_{P,N} \approx \frac{g_{mN5,13} + g_{m1,7}}{[1 + r_o g_{mN0,6}]g_{mN5,13}g_{mN1,7}} \tag{21}$$

and the output resistance of port Z could be gotten as

$$R_Z = g_{mP2}r_o^2 \| g_{mN10}r_o^2\,. \tag{22}$$

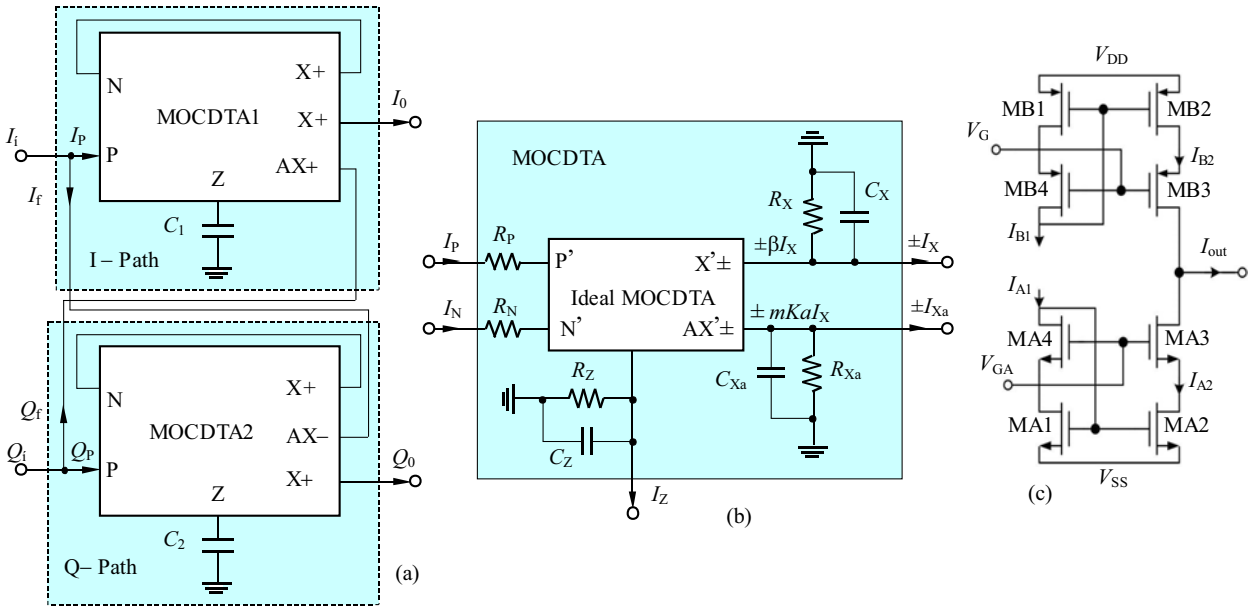

Fig. 4. (a) — the proposed polyphase filter using MOCDTA; (b) — MOCDTA with parasitic resistances and parasitic capacitors; (c) — the cascade current mirror of OTC's output stage

3.2 Operational Transconductance Circuit

Based on [36], a high-speed voltage-tunable operational transconductance circuit (OTC) shown in Fig. 3(c) has been proposed. MN16-MN21 consist of the linear differencing input stage, and MN22-MN29 consist of the output stage. The relation between $I_1 - I_2$ and V_Z could be gotten as

$$I_1 - I_2 = 2Gm(V_C - V_{SS} - 2V_{TH})V_Z = g_m V_Z \qquad (23)$$

where $Gm = \mu_n C_{ox} W/L$. According above equation, g_m could be adjusted linearly by external controlling voltage V_C. According to [37], μ_n and V_{TH} are affected by the temperature. When temperature increases, μ_n and V_{TH} could increase, which means Gm and V_{TH} will increase. It would make transconductance of OTC remain unchanged nearly with variational temperature.

The output stage of OTC is the low-voltage cascade current mirror which could achieve high output impedance, and the output resistance R_X could be written by

$$R_X \approx g_{mN29,28} r_{oN29,28} r_{oN27,26}\,. \qquad (24)$$

3.3 MOCDTA configuration

The MOCDTA is made up of three principal building blocks which are current differencing circuit, operational transconductance circuit, and current gain circuit. The MOCDTA realize current differencing function and current gain function, and has lower input resistance and higher output resistance. Besides, especially, the MOCDTA possesses low supply voltage and wide frequency characteristics. Fig. 3(d) shows the detail configuration.

In Fig. 3(d), the OTC1 with a polysilicon resistor R_{poly} that consist of the current gain circuit realizes the current gain function, and the current gain Ka introduced in (17) could be defined as

$$Ka = 2\alpha(L/W_{Rpoly} Gm(V_C - V_{SS} - 2V_{TH}) = 2\alpha(L/W)_{Rpoly} g_{ma} \qquad (25)$$

where, α is proportional to the ratio of doping density to thickness of the polysilicon, $(W/L)_{Rpoly}$ is the width to length ratio of the transistor polysilicon resistor R_{poly}, g_{ma} is transconductance of the OTC1. The resistor R_{poly} could be realized by MOS transistors in triode region or diode-connected MOS transistors. With (18) and (23), the main ports characteristics of MOCDTA could be rewritten as

$$(\alpha_{Pa} I_P - \alpha_{Na} I_N) Z_Z g_m = I_{X\pm}\,,\; KaI_{X\pm} = I_{Xa+}\,. \qquad (26)$$

4 THE PROPOSED POLYPHASE FILTER

4.1 Realization of the polyphase filter

The structure of the proposed first polyphase filter is shown in Fig. 4(a). From the Fig. 4(a), we can get the relation between I_P and I_O in I-path, which could be written as

$$\frac{I_o}{I_P} = \frac{1}{1 + j\omega C_1(1/g_{m1})} \qquad (27)$$

where g_{m1} is the transconductance of MOCDTA1. Likewise, Q_O and Q_P of the Q-path has the same relation. According to (27), each path performs a low-pass filter, and the polyphase filter could be realized by the cross-coupling of the two low-pass filter. The cut-off frequency of low-pass filters in each path could be gotten as

$$\omega_{01} = \frac{g_{m1}}{C_1}\,, \quad \omega_{02} = \frac{g_{m2}}{C_2} \qquad (28)$$

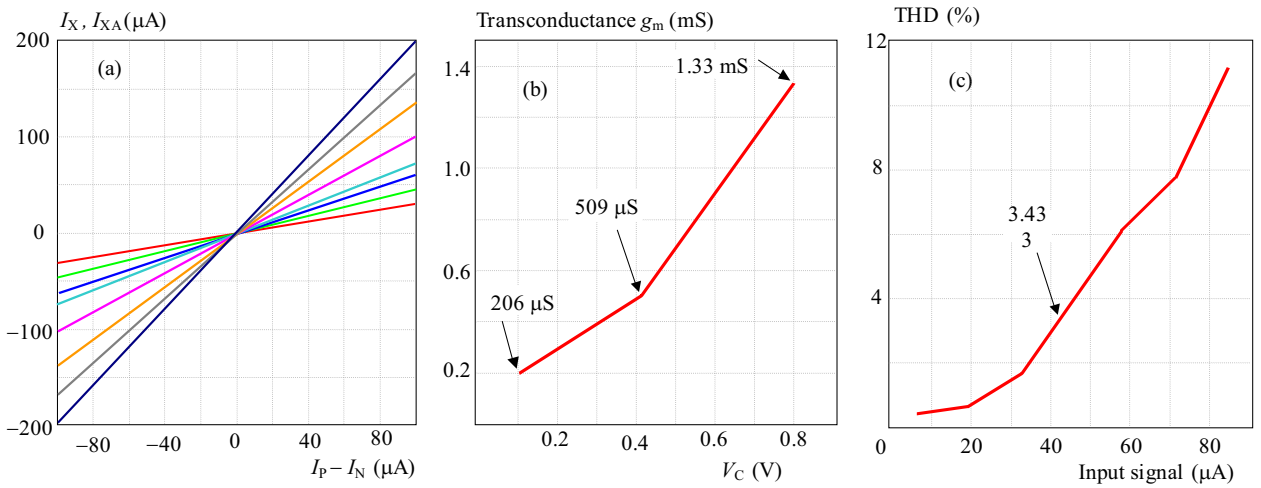

Fig. 5. (a) — DC response of port current of the MOCDTA; (b) — transconductance of the MOCDTA; (c) — total harmonic distortion of the MOCDTA

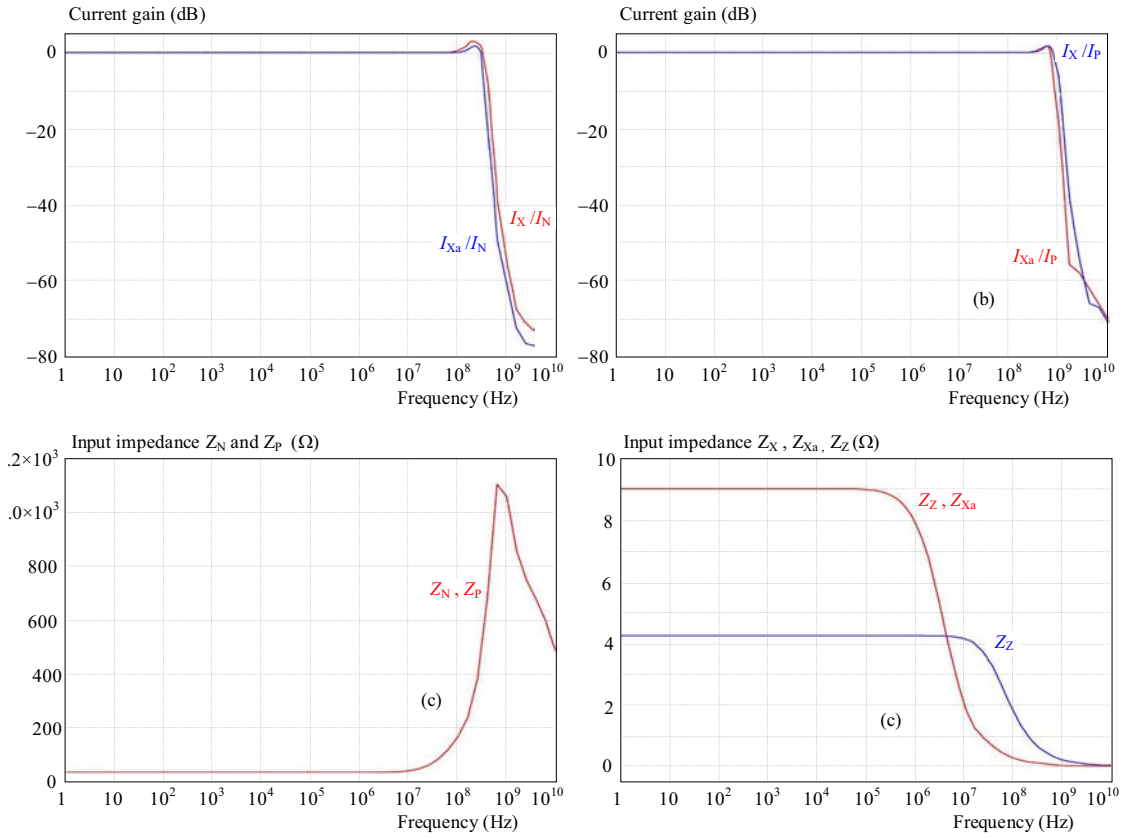

Fig. 6. (a) — AC response from port X, AX to N; (b) — AC response from port X, AX to P; (c) — input impedance of MOCDTA; (d) — output impedance of MOCDTA

where ω_{01} and ω_{02} are the cut-off frequencies of low-pass in two paths.

In Fig. 4(a), the feedback coefficient ω_C/ω_0 between two paths could be got. They are written as

$$\frac{\omega_{C1}}{\omega_{01}} = Ka_1\,, \quad \frac{\omega_{C2}}{\omega_{02}} = Ka_2 \tag{29}$$

where ω_{C1}/ω_{01} is the feedback from AX- of Q-path to I-path, and ω_{C2}/ω_{02} is the feedback from AX+ of I-path to Q-path.

From Fig. 1(c), the input and output matrix could be written by

$$\begin{bmatrix} I_i \\ Q_i \end{bmatrix} = \begin{bmatrix} 1 + j\omega/\omega_{01} & \omega_{C1}/\omega_{01} \\ -\omega_{C2}/\omega_{02} & 1 + j\omega/\omega_{02} \end{bmatrix} \begin{bmatrix} I_o \\ Q_o \end{bmatrix}. \tag{30}$$

Substituting (28) and (29) in (30), we can rewrite (30) as

$$\begin{bmatrix} I_i \\ Q_i \end{bmatrix} = F_1 \begin{bmatrix} I_o \\ Q_o \end{bmatrix} \tag{31}$$

where

$$F_1 = \begin{bmatrix} \left(\frac{\alpha_{N1}}{\alpha_{P1}}\right)\left(1+\frac{j\omega C_1}{\beta_1\alpha_{N1}g_{m1}}\right) & \mu_1 Ka_1 \\ -\mu_2 Ka_2 & \left(\frac{\alpha_{N2}}{\alpha_{P2}}\right)\left(1+\frac{j\omega C_2}{\beta_2\alpha_{N2}g_{m2}}\right) \end{bmatrix} \tag{32}$$

where $\alpha_P = 1--\varepsilon_P$, ε_P ($|\varepsilon_P| \ll 1$) denotes the current tracking error from ports P to Z; $\alpha_N = 1-\varepsilon_N$, ε_N ($|\varepsilon_N| \ll 1$) denotes the current tracking error from ports N to Z. β is the transconductance inaccuracy factor from ports Z to X. μ_2 and μ_1 is the inaccuracy factors from ports AX± to Z.

The (31) could be rewritten by

$$\begin{bmatrix} I_o \\ Q_o \end{bmatrix} = \frac{1}{|F_1|} A \begin{bmatrix} I_i \\ Q_i \end{bmatrix} \tag{33}$$

where

$$A = \begin{bmatrix} \frac{j\omega C_2+\beta_2\alpha_{N2}g_{m2}}{\beta_2\alpha_{P2}g_{m2}} & \mu_2 Ka_2 \\ \mu_1 Ka_1 & \frac{j\omega C_1+\beta_1\alpha_{N1}g_{m1}}{\beta_1\alpha_{P1}g_{m1}} \end{bmatrix}, \tag{34}$$

$$|F_1| = \frac{(j\omega C_1+\beta_1\alpha_{N1}g_{m1})(j\omega C_2+\beta_2\alpha_{N2}g_{m2})}{\beta_1\beta_2\alpha_{P1}\alpha_{P2}g_{m1}g_{m2}} + K \tag{35}$$

where $K = \mu_1\mu_2 Ka_1 Ka_2$.

The transfer function H_{1p} and the mismatch function H_{1m} have been defined in [11], which are written as

$$H_{1p}(j\omega) = (1/|F_1|)[(A_{11}+A_{22})/2 - j(A_{12}-A_{21})/2], \tag{36}$$

$$H_{1m}(j\omega) = (1/|F_1|)[(A_{11}-A_{22})/2 - j(A_{12}-A_{21})/2] \tag{37}$$

where A_{11}, A_{12}, A_{21}, and A_{22} are the elements of the matrix A.

In ideal polyphase filter, there are $C_1 = C_2 = C$, $g_{m1} = g_{m2} = g_m$, and $Ka_1 = Ka_2 = Ka$. The transfer function H_{1p} is written as

$$H_{1p}(j\omega) = \{j\omega C(\beta_1\alpha_{P1}+\beta_2\alpha_{P2}) + \beta_1\beta_2\alpha_{N2}\alpha_{P1}g_m + \beta_1\beta_2\alpha_{N1}\alpha_{P2}g_m\} \times \frac{1}{2|F_1|\beta_1\beta_2\alpha_{P1}\alpha P2 g_m} + \frac{K_1 j}{|F_1|} \tag{38}$$

where $K_1 = (\mu_1 Ka_1 + \mu_2 Ka_2)/2$. The mismatch function H_{1m} could be written as

$$H_{1m}(s) = \{sC(\beta_1\alpha_{P1}-\beta_2\alpha_{P2}) + \beta_1\beta_2\alpha_{N2}\alpha_{P1}g_m - \beta_1\beta_2\alpha_{N1}\alpha_{P2}g_m \times \frac{1}{2|F_1|\beta_1\beta_2\alpha_{P1}\alpha_{P2}g_m} + \frac{K_2 j}{|F_1|} \tag{39}$$

where $K_2 = (\mu_1 Ka_1 - \mu_2 Ka_2)/2$.

With ideal conditions $\alpha_{N1} = \alpha_{N2} = \alpha_{P1} = \alpha_{P2} = 1$, $\beta_1 = \beta_2 = 1$, and $\mu_1 = \mu_2 = 1$, the transfer function H_{1p} could be simplified into

$$H_{1pi} = \frac{1}{j[\omega(C/g_m) - Ka] + 1} \tag{40}$$

and the mismatch function H_{1m} could be simplified into H_{1mi}, which could be written as: $H_{1mi} = 0$. (41)

Substituting (40) in (3), the IRR of the proposed first polyphase filter is written by

$$IRR(j\omega) = \left|\frac{g_m - jKag_m - jC\omega}{g_m - jKag_m + jC\omega}\right| \tag{42}$$

according to the (42), the IRR at frequency ω_C could be get, which is written as

$$IRR(\omega_C) = \sqrt{1+4Ka^2} \tag{43}$$

so, the IRR could be adjusted by Ka with constant ω_0. This is to say, the IRR and cut-off frequency could be adjusted independently.

According to (28) and (29), in the ideal condition, ω_C could be tuned in wide range with constant ω_0 through adjusting Ka. The quality factor Q of the filter is $\omega_C/2\omega_0$ which is equal to $Ka/2$, it would be influenced by temperature due to transconductance g_{ma} according to (25), and the relation between transconductance and temperature is introduced in Sec. 3.2.

According to Fig. 4(a), the input impedance of the polyphase filter is $R_{P,N}//R_X$. Because of $R_X \gg R_{P,N}$, the input impedance could be $R_{P,N}$ which is very low. Besides, the output impedance is R_X which is very high. Based on above two points, the polyphase filter is suitable to connecting to external circuits.

4.2 Analysis with parasitic parameters

The following of non-ideal characteristics are discussed from the perspectives of parasitics. The simplified equivalent circuit of the non-ideal MOCDTA model is shown in Fig. 4(b).

As the Fig. 4(b) depicts, there are parasitic resistances (R_P and R_N) at input terminals P and N, and parasitic resistances and capacitors (R_Z, C_Z, R_X, C_X, and R_{Xa}, C_{Xa}) from terminal Z, X±, and Xa± to ground. In order to simplify the discussion, the parasitic impedances at terminals of MOCDTA1 are taken to be same with the ones at corresponding terminals of MOCDTA2. Considering the parasitic parameters, the transfer function of the polyphase filter would be rewritten by

$$H_{pp}(j\omega) = \frac{\alpha_P\beta g_m R_A}{s(C+C_Z-j\alpha_P\mu Ka\beta g_m R_A + \alpha_N\beta g_m R_B + 1/R_Z} \tag{44}$$

where

$$R_A = \frac{1}{1+R_P/R_{Xa}+sC_{Xa}R_P}, \tag{45}$$

$$R_B = \frac{1}{1+R_N/R_X+sC_X R_N}. \tag{46}$$

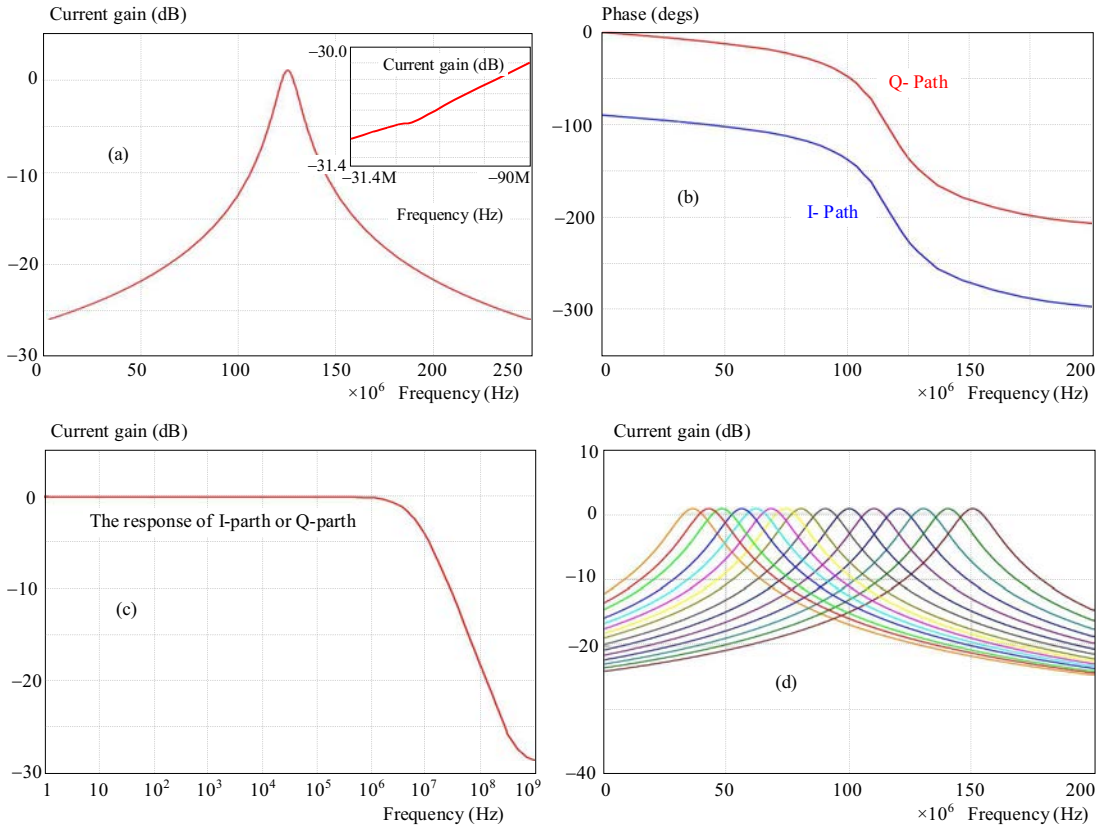

Fig. 7. (a) — the amplitude-frequency response of the proposed polyphase filter; (b) — the phase characteristics of the two paths; (c) — the amplitude-frequency response of I-path or Q-path; (d) — the amplitude-frequency responses of the proposed polyphase filter with different ω_C

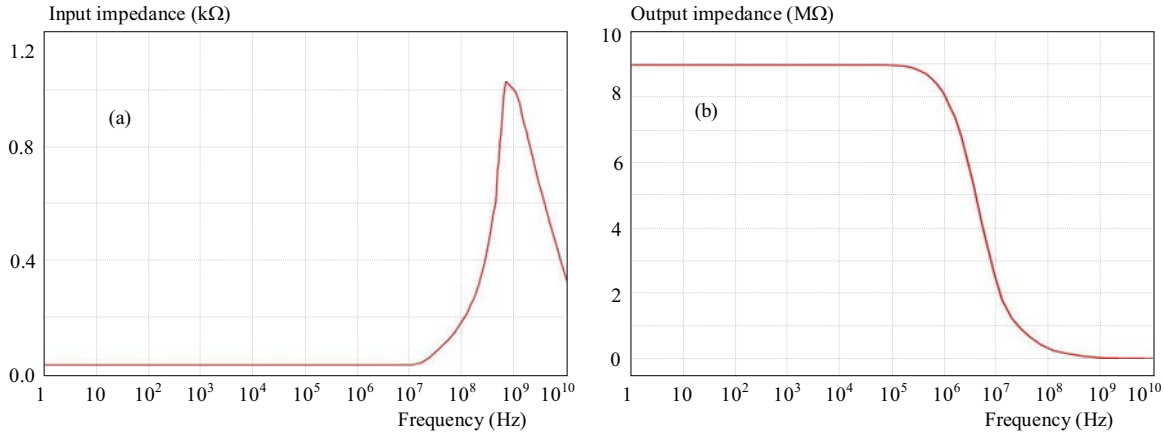

Fig. 8. The impedance of the proposed filter: (a) — input impedance; (b) — output impedance

It is easily observed that the parasitic capacitors C_Z could be absorbed into the external capacitor C and the parasitic resistor R_Z at terminal Z would change the type of the impedance which should be of a purely capacitive character. Besides, according to (44), the magnitude of the amplitude-frequency response' apex would not be 1 (0 dB) whose value is written as

$$|H_{pp}(j\omega_C)| = \frac{\alpha_P \beta g_m R_A}{\alpha_N \beta g_m R_B + 1/R_Z}\,. \tag{47}$$

The cut-off frequency and centre frequency could be rewritten by

$$\omega_0 = \frac{1/R_Z + \alpha_N \beta g_m R_B}{C}\,, \tag{48}$$

$$\omega_C = \frac{\alpha_P \beta \mu g_m K a R_A}{C}\,. \tag{49}$$

So, both the centre frequency ω_C and cut-off frequency ω_0 are affected by the parasitic parameters, and a good design for MOCDTA is necessary.

The sensitivities of the curt-off frequency ω_0 to the non-idealities and external components are gotten by

$$\begin{aligned} S^{\omega_0}_{\alpha_N,\beta,g_m} &= \frac{\alpha_P\beta R_B gm}{1/R_Z + \alpha_P\beta R_B gm} < 1\,, \\ S^{\omega_0}_{R_Z} &= \frac{-1}{1 + R_Z\alpha_P\beta R_B gm} > -1\,, \\ S^{\omega_0}_{C} &= -1\,, \qquad S^{\omega_0}_{R_{Xa},C_{Xa},R_P,Ka,\mu} = 0 \end{aligned} \tag{50}$$

due to

$$S^{A}_{R_N,C_X} < 1\,, \quad S^{A}_{R_X} > -1\,. \tag{51}$$

So

$$\left|S^{\omega_0}_{R_N,C_X,R_X}\right| < 1\,. \tag{52}$$

With the same analysis, the sensitivities of the centre frequency ω_C to the non-idealities and external components are written by

$$\begin{aligned} S^{\omega_C}_{\alpha_P,\beta,\mu,g_m,Ka} = 1\,, \quad S^{\omega_C}_{C} = -1\,, \\ \left|S^{\omega_C}_{R_{Xa},R_P,C_{Xa}}\right| < 1\,, \quad S^{\omega_C}_{R_X,C_X,R_N,\alpha_N,R_Z} = 0\,. \end{aligned} \tag{53}$$

4.3 Harmonic distortion of the proposed polyphase filter

The proposed polyphase filter is comprised of two MOCDTAs which would product harmonic distortion. As previously depicted, CDC and OTC is made up of MOCDTA. In CDC, due to the negative feedback in two input stages that achieved by $MN0$, $MN5$ and $MN6$, $MN13$, the harmonic distortion is dampened to some extent. Moreover, the low-pass response (band-pass response is obtained as considering the feedback between two paths), achieved due to the process that current signal $I_Z = I_P - I_X$ from CDC pass through the external capacitor and OTC, would filter the harmonic generated by CDC. So, the OTC impacts the nonlinearity of MOCDTA mainly. The OTC consists of transconductance portion and cascade current mirror portion. As (23) shows, the good linearity between the differential output current and the input voltage in the transconductance portions could be got, which means the nonlinearity influenced by the cascade current mirror portion need to be considered mainly.

Let us consider the output stage of OTC which is comprised of cascade current mirror portion. We could assume a sinusoidal input current $i_{\rm in} = I_M \sin(\omega t)$, and the output current can be expressed as

$$i_{\rm out}0(t) = a_0 + a_1 i_{\rm in} + a_2 i_{\rm in}^2 + a_3 i_{\rm in}^3 \tag{54}$$

where a_0 is an offset current and a_1 is the mirror ratios since around the quiescent point is $\Delta i_{A1} = -\Delta i_{B1} = i_{\rm in}/2$. a_2 and a_3 are mirror efficient for the second-order and third-order harmonic, and the approach to calculating a_2 and a_3 is proposed in [38]. Taking the derivative of $i_{\rm out}$ with respect to $i_{\rm in}$, evaluated at the maximum and minimum input signal ($+I_M$ and $-I_M$), HD_2 and HD_3 are given by

$$HD_2 = \frac{1}{2}\frac{a_2}{a_1} I_M \approx \frac{1}{2} a_2 I_M = \frac{1}{8}\Big(\frac{\partial i_{A2}}{\partial i_{A1}}\Big|_{I_M} - \frac{\partial i_{B2}}{\partial i_{B1}}\Big|_{I_M}\Big), \tag{55}$$

$$HD_3 = \frac{1}{4}\frac{a_3}{a_1} I_M^2 \approx \frac{1}{4} a_3 I_M^2 = \frac{1}{24}\Big(\frac{\partial i_{A2}}{\partial i_{A1}}\Big|_{I_M} + \frac{\partial i_{B2}}{\partial i_{B1}}\Big|_{I_M} - \frac{\partial i_{A2}}{\partial i_{A1}}\Big|_{I_Q} - \frac{\partial i_{B2}}{\partial i_{B1}}\Big|_{I_Q}\Big) \tag{56}$$

where I_Q is the quiescent current of the output branch.

The output stage of OTC is shown in Fig. 4(c) separately. Without loss of generality, we just consider the n-type cascade mirror MA ($MA1 - MA3$), and assume transistors $MA1 - MA3$ to be ideally matched and to have the same transconductance gain. The V_{GA} could be given by

$$V_{GA} = V_{DS2} + V_{GS3} \approx 2V_{TN} + 2\sqrt{\frac{I_Q}{K_N}} \tag{57}$$

where I_Q is the quiescent current, K_N is $(1/2)\mu C_{OX}$ (W/L), V_{TN} is the threshold voltage of NMOS, V_{DS2} is the drain-source voltage of $MA2$, and V_{GS3} is the gate-source voltage of $MA3$. So, with (57) there are

$$\begin{aligned} i_{A2} &= \frac{1 + \lambda_N(V_{GA} - V_{GS3})}{1 + \lambda_N V_{GS1}} i_{A1} \\ &\approx \Big[1 + \frac{2\lambda_N}{\sqrt{K_N}} \frac{\sqrt{I_Q} - \sqrt{i_{A1}}}{1 + \lambda_N\big(V_{TN} + \sqrt{\frac{i_{A1}}{K_N}}\big)}\Big] i_{A1} \end{aligned} \tag{58}$$

where $\lambda_?$ is the channel-length modulation coefficient. Besides, there is

$$\lambda_N\Big(V_{TN} + \sqrt{\frac{i_{A1}}{K_N}}\Big) \ll 1 \tag{59}$$

so, we can get

$$\frac{\partial i_{A2}}{\partial i_{A1}} \approx 1 + \frac{2\lambda_N}{\sqrt{K_N}}\Big(\sqrt{I_Q} - \frac{3}{2}\sqrt{i_{A1}}\Big). \tag{60}$$

Following the same steps for the p-type current mirror $MB1 - MB3$, and assuming the transconductance gain to be equal for both current mirrors (ie $K_N = K_P = K$). Substituting (60) into (55) and (56), we can get

$$HD_2 \approx \frac{\lambda_N - \lambda_P}{4}\sqrt{\frac{I_Q}{K}}\Big(\frac{3}{2}\sqrt{\frac{I_M}{I_Q} - 1}\Big), \tag{61}$$

$$HD_3 \approx \frac{\lambda_N + \lambda_P}{8}\sqrt{\frac{I_Q}{K}}\Big(\sqrt{\frac{I_M}{I_Q} - 1}\Big) \tag{62}$$

so, harmonic distortion HD_3 and HD_2 depend on the relative magnitude of the input signal and λ_N and λ_P. With ideally matched transistors and equal transconductance gain, the harmonic distortion HD_2 could be very low. So, third-order harmonic distortion HD_3 is the dominant contribution, and we can reduce it by increasing the transconductance gain and the channel length of the transistors.

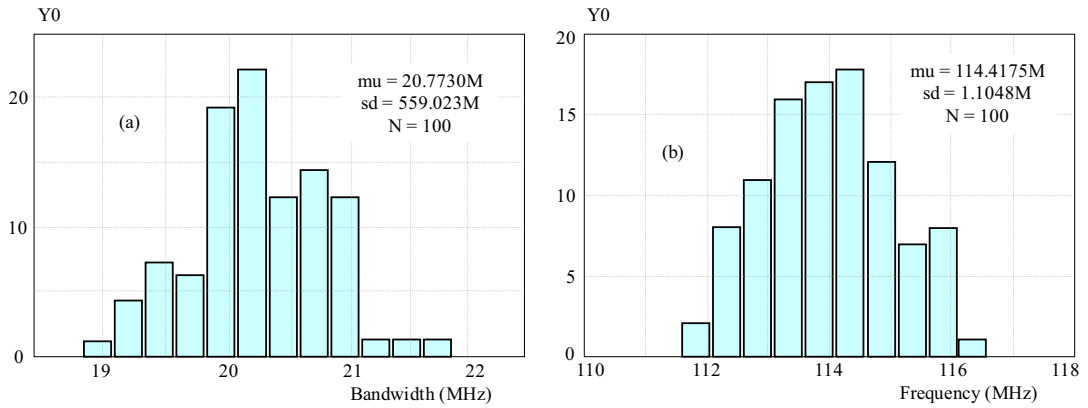

Fig. 9. Monte-carlo analysis of Parameters: (a) — Bandwidth; (b) — center frequency

Table 1. Comparison with polyphase filter using other active components

Spec.	order	Centre frequency (MHz)	Bandwidth (MHz)	IRR (dB)	Active components' number	Resistors' number	Capacitors' number	Power (V/mW)
This work	1	114	11.1	31.6	MOCDTA/2	0	2	±0.8/4.48
[1]	1	< 5	NA	15	CCII/4	6	2	NA
[6]	5	0.25	0.22	64	OPAMP/2	8	4	5/NA
[10]	1	0.135	0.018	> 20	CCCII/2	2	2	±1.5/NA
[11]	1	< 60	NA	> 11	CDBA/2	6	2	±2.5/NA
[13]	6	2	1	> 45	Gm-C/36	0	24	2.7/12.7
[14]	7	3	1	> 53	Gm-C/14	0	6	2.3/7.36
[15]	5	5	8	> 40	OTA/5	21	18	3/14
[16]	4	0.5	0.9	28	OTA/16	0	0	1.8/1.98
[17]	4	2.5	3.6	31.5	OTA/4	4	2	2.4/2.45
[21]	1	1	0.83	NA	FDCC/4	12	4	±1.5/3.6
[23]	1	3	1	> 54 (6^{th}	CF/2	2	2	±1.35/2.38
[26]	1	1.9	1.9	> 60 (6^{th}	CFOA/3	8	2	1.5/5.6

5 SIMULATION RESULTS

5.1 Simulation of MOCDTA

The whole proposed circuits have been simulated by Spectre Simulation in CHRT 0.18 μm standard CMOS process. The supply voltage are $VDD = -VSS = 0.8$ V, and the bias current used in CDC is $I_{BB} = 100$ uA. The value of the polysilicon resistor R_{poly} is 3.2 kΩ.

The DC transfer characteristic of MOCDTA which is given in Fig. 5(a) shows a very good performance. In Fig. 5(a), when the $I_P - I_N$ changes from -100 uA to 100 uA with V_C changes from 0 V to 800 mV and $V_{Ca} = 0.2$ V ($Ka = 1$), the X ports current I_X and AX ports current I_{Xa} be varied linearly. ($R_Z = 1.5$ K).

Figure 5(b) shows the variation range of transconductance of the MOCDTA. When V_C changed from 0.1 V to 0.8 V, the transconductance from port Z to port X± of MOCDTA vary linearly in two ranges which are from 1.33 mS to 509 μS and from 509 μS to 206 μS.

For the study of the circuit's harmonic distortion under different amplitude input signals, circuit's total harmonic distortion (THD) figure (sinusoidal current at 10 kHz as input signal, it amplitude changes within the range from 5 μA to 75 μA) is shown in Fig. 5(c). It is easy to know that the circuit's THD is less than 3 % when current does not exceed 35 μA.

Figures 6(a) and 6(b) depict the AC transfer characteristics of MOCDTA. During the simulation, the external resistance at Z port is $R_Z = 1.5$ K, external bias voltages are $V_C = 0.5$ V for the first OTC and $V_{Ca} = 0.2$ V for the second OTC. In Figs. 6(a) and 6(b), the current transfer ratios α_P, α_N and transconductance g_m for the first OTC and g_{ma} for the second OTC are found to be 1.02, 1.002, 672 μS, and 310 μS. When the frequency is over 853 MHz, the amplitudes of these responses reduce over -3 dB.

Figure 6(c) illustrates the low input impedance of MOCDTA, and Fig. 6(d) denotes the high output impedance of MOCDTA. In Fig. 6(c), the impedance of the input ports P and N are both 31.2 Ω. It is clear that the output impedance of ports X± and Xa± are both 9.1 MΩ and the one of ports Z is 4.28 MΩ in Fig. 6(d).

5.2 Simulation of the polyphase filter

With ±0.8 V supply, the proposed polyphase filter has been simulated. It has been designed with $C_1 = C_2 =$

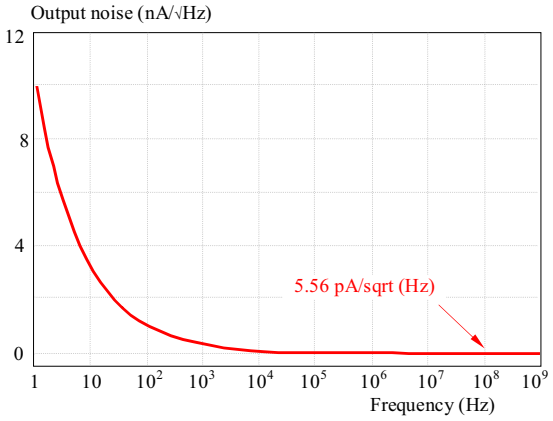

Fig. 10. Output noise of the filter

5.5 pF, $V_C = 100$ mV, and $V_{Ca} = 600$ mV. In the above conditions, the low-pass filters in each path are equal, and they are cross-coupling to realize the polyphase filter. The phases of input signals are different by 90 degs, and their amplitudes are equal. The amplitude-frequency responses of the I-path and Q-path which are equal each other are shown in Fig. 7(a), and the amplitude-frequency response near $-\omega_C$ is shown in the upper right of Fig. 7(a). In Fig. 7(a), the centre frequency of the polyphase filter could be 114 MHz. The bandwidths are obtained with 11.1 MHz. The filter could achieve 0.7 dB gain at ω_C, and achieve -30.9 dB gain at $-\omega_C$. So, the IRR is obtained with 31.6 dB. In Fig. 7(b), it is observed that the output signals possess 90-degs phase difference as input signals.

The amplitude-frequency response of low-pass filter in I-path or Q-path without the feedback between I-path and Q-path is shown in Fig. 7(c), and their bandwidths are both 5.8 MHz which are almost half of the bandwidth of polyphase filter. It means that the low-pass amplitude-frequency response in Fig. 7(c) is shifted as band-pass amplitude-frequency response in Fig. 7(a) by the cross-coupling.

With $C_1 = C_2 = 2.5$ pF, $V_C = 210$ mV, and V_{Ca} changes from 100 mV to 800 mV by 50 mV, the amplitude-frequency responses is shown in Fig. 7(d). It is clear that the centre frequency could be tuned from 38 MHz to 150 MHz. During the change, the IRR and the centre frequency are increasing meanwhile the bandwidths keep 20.1 MHz.

The proposed filter possesses low input impedance and high output impedance which are shown in Fig. 8. In Fig. 8(a) and Fig. 8(b), it is observed that the input impedance and output impedance are almost equal to the ones of MOCDTA.

The bandwidth and center frequency have been operated by Monte-carlo analysis which consider process and mismatch. There are 100 samples per each analysis. The analysis results are shown in Fig. 9. In Fig. 9, the average of bandwidth is 20.8 MHz, and its mean-square deviation is 559.0 KHz. So the deviation range is 2.7 %. The average of center frequency is 114.4 MHz, and its mean-square deviation is 1.1 MHz. The deviation range is 0.097 %.

The output noise is concerned, and the simulation results are shown in Fig. 10. The results show that the output noise presents a low value over the entire passband. The output noises of the filter are both 5.56 pA/sqrt(Hz) at 114 MHz, So, the output noise is even lower within the bandwidth.

Compared with the polyphase filter using the OTA, the polyphase filter using MOCDTA has advantages in working at the high centre frequency. In terms of the IRR and bandwidth, we can find that the proposed first-order polyphase filter is comparable with other high-order polyphase filters. Table 1 includes the comparison with recent polyphase filters using other components. It can be seen that the structure of the proposed filter are less complicated than the ones of the others in Table 1 meanwhile the proposed filter could obtain comparable IRR with low supply voltage. Besides, the centre frequency of the proposed filter is higher than others' one.

6 CONCLUSION

In this paper, two new active current-mode polyphase filters were presented. The proposed filter has following advantages. The first, the proposed polyphase filter whose structure is simple just is comprised of two MOCDTAs and two capacitors. The second, this filter can work at a high frequency without a complicated circuit whose centre frequency vary from 38 MHz to 150 MHz by adjusting external bias voltage V_{Ca}. The third, the proposed filter possesses low input impedance and high output impedance which is suitable for cascade. The forth, all capacitors are grounded which is fit for IC technology. The fifth, the bandwidth and centre frequency could be adjusted independently by external bias voltage V_C and V_{Ca}. The above properties have been well verified by the simulation.

Acknowledgments

This work was supported in part by the National Natural Science Foundation of China (No. 61274020).

References

[1] ABUELMA'ATTI, A.—ABUELMA'ATTI, M. T.: A New Active Polyphase Filter for Image Rejection Using Second Generation Current Conveyors, Proc. the 9th International Conf. on Circuits, 2005, pp. 1–4.

[2] HARTLEY, R.: Single-Sideband Modulator, U.S. Patent 1666206, April, 1928.

[3] WEAVER, D.: A Third Method of Generation and Detection of Single-Sideband Signals, Proc. IRE (1956), 1703–1705.

[4] RAZAVI, B.: RF Microelectronics, Prentice hall, U.S.A, 1998.

[5] HORNAK, T.: Using Polyphase Filters as Image Attenuators, RF Design **6** (2001), 26–34.

[6] HADDAD, F.—ZAÏD, L.-FRIOUI, O.: Polyphase Filter Design Methodology for Wireless Communication Applications, INTECH Open Access Publisher, 2010.

[7] CROLS, J.—STEYAERT, M.: An Analog Integrated Polyphase Filter for High Performance Low-IF Receiver, Proc. VLSI Circuits, 1995, pp. 87–88.

[8] SEDRA, A.—SNELGROVE, W.—ALLEN, R.: Complex Analog Bandpass Filters Designed by Linearly Shifting Real Low-Pass Prototypes, Proc. IEEE Int. Symp. on Circuits and Systems, 1985, pp. 1223–1226.

[9] MINNIS, B.—MOORE, P.: Non-Complex Signal Processing in a Low-IF Receiver, IEE Proceedings-Circuits, Devices and Systems **149** (2002), 322–330.

[10] SHAHRANI, S.—GAHTANI, M.: A New Polyphase Current-Mode Filter Using Digitally-Programmable CCCII, Proc. 18th Int. Conf. on Micro-electronics ICM, 2006, pp. 142–145.

[11] SAGBAS, M.: Design of CDBA-based Active Polyphase Filter for Low-IF Receiver Applications, Turk. J. Elec. Eng. & Comp. **19** (2011), 565–574.

[12] STIKVOORT, E.: Polyphase Filter Section with OPAMPs, IEEE Transactions on Circuits and Systems-II: Analog and Digital Signal Processing **50** (2003), 376–378.

[13] EMIRA, A.—SÁNCHEZ-SINENCIO, E.: A Pseudo Differential Complex Filter for Bluetooth with Frequency Tuning, IEEE Trans. Circuits Syst. II, Analog. Digit. Signal Process **50** (2003), 742–754.

[14] ANDREANI, P.—MATTISSON, S.—ESSINK, B.: A CMOS gm-C Polyphase Filter with High Image Band Rejection, Proc. The European Solid State Circuits Conf., 2000, pp. 244–247.

[15] NOTTEN, M.—BREKELMANS, H.—RAMBEAU, V.: A 5th Order 14 mWatt Active Polyphase Filter for Analog and Digital TV on Mobile Applications, Proc. IEEE Solid-State Circuits Conf., 2006, pp. 211–214.

[16] ZHOU, M.: A Tunable Gm-C Polyphase Filter with High Linearity and Automatic Frequency Calibration, IEICE Electronics Express **11** (2014), 1–6.

[17] LIU, S.: A New Fourth-Order Gm-C CMOS Polyphase Filter for Low-IF Receiver, Proc. 2012 IEEE 11th Int. Conf., 2012, pp. 1–3.

[18] LAOUDIAS, C.—PSYCHALINOS, C.: Low-Voltage Bluetooth/ZigBee Complex Filter Using Current Mirrors, Proc. ISCAS, May 2010, pp. 1268–1271.

[19] LAOUDIAS, C.—PSYCHALINOS, C.: 1.5 V Complex Filters Using Current Mirrors, IEEE Transactions on Circuits and Systems II **58** (2011), 575–579.

[20] ZHANG, X.—KAMBAYASHI, N.—SHINADA, Y.: A Realization of Active Current-Mode Resonator with Complex Coefficients Using CCIIs, IEICE Transactions on Fundamentals **80** (1997), 413–415.

[21] SOLIMAN, E.—MAHMOUD, S.: New CMOS fully differential current conveyor and its application in realizing sixth order complex filter, Pro. The IEEE Int. Symposium on Circuits and Systems, May,.

[22] ABUELMA'ATTI, M.—AL-SHAHRANI, S.: A New Polyphase Current-Mode Filter Using Programmable-Gain Current-Controlled Current-Conveyor, WSEAS Trans. Electron **2** (2005), 138–141.

[23] ALZAHER, H.—TASADDUQ, N.: A CMOS Low Power Current-Mode Polyphase Filter, Proc. IEEE Int. Symp. On Low Power Electronics Design, 2009, pp. 75–79.

[24] UN, M.: Implementation of Polyphase Filter Section with CFAs, Frequenz **58** (2004), 221–224.

[25] UN, M.: Analysis of Polyphase Filter Section with CFAs, WSEAS Trans. on CAS **2** (2003), 421.

[26] SAMIOTIS, P.—PSYCHALINOS, C.: Low-Voltage Complex Filters Using Current Feedback Operational Amplifiers, ISRN Electronics (2013), 1–7.

[27] TOUMAZOU, C—LIDGEY, F.-HAIGH, D.: Analogue IC Design: The Current Mode Approach, Presbyterian Publishing Corp., London, 1990.

[28] ALZAHER, H.—TASADDUQ, N.—AL-AMMARI, F.: Optimal Low Power Complex Filters, IEEE Transactions on Circuits and Systems I **60** (885–895).

[29] GUO, C.: A Fully-Integrated 900-MHz CMOS Wireless Receiver with On-Chip RF and IF Filters and 79-dB Image Rejection, IEEE Solid-State Circuits **37** (2001), 1084–1089.

[30] BIOLEK, D.: CDTA-Building Block for Current-Mode Analog Signal Processing, Proc. The ECCTD03, Poland, 2003, pp. 397–40000.

[31] HASSAN, M.—PAUL, S.: A New Current Mode Quadrature Oscillator using Current Differencing Transconductance Amplifier (CDTA), Journal of VLSI Design Tools & Technology **4** (2014), 39–42.

[32] JIN, J.—WANG, C.: CDTA-Based Electronically Tunable Current-Mode Quadrature Oscillator, International Journal of Electronics **101** (2014), 1086–1095.

[33] JANTAKUN, A.—JAIKLA, W.: Current-Mode Quadrature Oscillator Based on CCCDTAs with Noninteractive Dual-Current Control for Both Condition of Oscillation and Frequency of Oscillation, Turkish Journal of Electrical Engineering & Computer Sciences **21** (2013), 81–89.

[34] NORGAARD, D.: The Phase-Shift Method of Single-Sideband Signal Reception, Proc. the IRE, 1956, pp. 1735–1743.

[35] KAUKOVUORI, J.—STADIUS, K.: Analysis and Design of Passive Polyphase Filters, IEEE Transactions on Circuits and Systems I: Regular Papers **55** (2008), 3023–3037.

[36] BULT, K.—WALLINGA, H.: A class of analog CMOS circuits based on the square-law characteristic of an MOS transistor in saturation, IEEE Journal of Solid-State Circuits 22 (.

[37] ARORA, N.: Mosfet Models for VLSI Circuit Simulation, Springer-Verlag, Austria, 1993.

[38] SEDRA, A.—SMITH, K.: A Second-Generation Current Conveyor and its Applications, IEEE Trans. Circuit Theory **CT-17** (1970), 132–133.

Received 9 February 2016

Hao Peng received the BS degree in 2013. Now he is studying towards the MS degree at the Hunan University. His research includes design of current-mode integrated circuits.

Chunhua Wang was born in Yongzhou, China, in 1963. He received the PhD degree from Beijing University of Technology, Beijing, China. He is currently Professor of Hunan University, Changsha, China. His research includes current-mode circuit design, RFIC design. He is the corresponding author of this paper. Xiaotong Tian is studying towards the BS degree at the Hunan University.